International Journal of Nanomedicine

Dovepress

open access to scientific and medical research

Open Access Full Text Article

ORIGINAL RESEARCH

4D Thermo-Responsive Smart hiPSC-CM Cardiac Construct for Myocardial Cell Therapy

Sung Yun Hann[1,*], Haitao Cui[1,*], Timothy Esworthy[1], Lijie Grace Zhang[1–4]

[1]Department of Mechanical and Aerospace Engineering, The George Washington University, Washington, DC, 20052, USA; [2]Department of Electrical and Computer Engineering, The George Washington University, Washington, DC, 20052, USA; [3]Department of Biomedical Engineering, The George Washington University, Washington, DC, 20052, USA; [4]Department of Medicine, The George Washington University, Washington, DC, 20052, USA

*These authors contributed equally to this work

Correspondence: Lijie Grace Zhang, Department of Mechanical and Aerospace Engineering, The George Washington University, Science and Engineering Hall 3590, 800 22nd Street NW, Washington, DC, 20052, USA, Tel +1 202 994 2479, Fax +1 202 994 0238, Email lgzhang@gwu.edu

Purpose: 4D fabrication techniques have been utilized for advanced biomedical therapeutics due to their ability to create dynamic constructs that can transform into desired shapes on demand. The internal structure of the human cardiovascular system is complex, where the contracting heart has a highly curved surface that changes shape with the heart's dynamic beating motion. Hence, 4D architectures that adjust their shapes as required are a good candidate to readily deliver cardiac cells into the damaged heart and/or to serve as self-morphing tissue scaffolds/patches for healing cardiac diseases. In this proof-of-concept in vitro study, a two-in-one 4D smart cardiac construct that integrates the functions of minimally invasive cell vehicles and in situ tissue patches was developed for repairing damaged myocardial tissue.

Methods: For this purpose, a series of thermo-responsive 4D structures with different shapes and sizes were fabricated via the combination of fused deposition modeling (FDM)-printing and stamping molding. The thermo-responsive 4D constructs were firstly optimized to exhibit their shape transformation behavior at the designated temperature for convenient control. After which, the mechanical properties, shape recovery rate, and shape recovery speed of the 4D constructs at different temperatures were thoroughly evaluated. Also, the proliferation and functional prototype of human-induced pluripotent stem cell-derived cardiomyocytes (hiPSC-CMs) on the 4D constructs were quantified and evaluated using F-actin staining and immunostaining.

Results: Our results showed that the 4D constructs possessed the desirable capability of shape-changing from spherical carriers to unfolded patches at human body temperature and exhibited excellent biocompatibility. Moreover, myocardial maturation in vitro with a uniform and printing pattern-specific cell distribution was observed on the surface of the unfolded 4D constructs.

Conclusion: We successfully developed a 4D smart cardiac construct that integrates the functions of minimally invasive cell vehicles and in situ tissue patches for repairing damaged myocardial tissue.

Keywords: 4D printing, shape memory, nanostructure, myocardial regeneration, cellularized patch, minimally invasive

Introduction

Based on the recent statistics of the American Heart Association and the Public Health Agency of Canada, heart diseases account for the most considerable portion of the annual deaths in North America.[1,2] Also, it was reported that approximately 18.7 million people in North America possess a potential risk of various heart diseases.[1–3] A universal cause of heart disease is acute myocardial infarction (MI), which is commonly known as a heart attack. Generally, MI results in irreversible cell loss and leads to myocardial thinning and left ventricular dilation.[4–6] The current clinical approaches for the treatment of MI, mainly rely on recanalizing the occluded coronary artery and preventing myocardial necrosis. Specifically, bypass graft surgery, angioplasty, or drug and thrombolytic therapies have been universally used.[7–9] However, these treatments, as well as acellularized cardiac patches, only temporarily relieve the symptoms associated with MI, but ultimately lead to incomplete repair of necrotic myocardial tissues.[7,10–12] Therefore, substantial biomedical research has been dedicated to regenerating engineered cardiac tissues using different approaches, such as 3D printing,[13] stem cell or growth factor injection,[14,15] porous biological scaffolds,[6] or

Received: 27 December 2022
Accepted: 1 April 2023
Published: 5 April 2023

injectable hydrogel and patches.[16–19] Especially, 3D printing has gained remarkable attention due to its reproducibility and versatility in the rapid fabrication of targeted tissue constructs in a biomimetic manner.[5,20–22] In particular, 4D printing has emerged in tissue engineering due to its adaptable ability to generate constructs that can change their external shape and functions when exposed to certain stimuli.[23–27] In our previous studies, we utilized a 4D printing technology to mimic the curved and dynamic structure of myocardial tissue to achieve seamless integration and improved mechanical stretchability.[5,25,28] Considering the features of myocardial tissues, 4D constructs that respond to their surrounding environment are more suitable than static nature, 3D printed structures.[29–31]

4D constructs are especially useful for the treatment of cardiovascular diseases as the curvature of the heart repeatedly transforms. Hence, static 3D constructs do not possess the capability to properly react to this dynamic condition. For example, static constructs require a thoracotomy for implantation, which is a complex and time-costly process, especially for MI treatments. However, minimally invasive 4D smart constructs offset this drawback. Also, cell transplantation is critical for MI therapy due to the insufficient regenerative capacity of damaged myocardial tissues. From the perspective of cell delivery, uncontrollable 3D static constructs would result in evident cell losses.[32,33] Therefore, the use of an intelligent-responsive 4D material for cardiovascular disease treatments is crucial.

Despite the progress of fabrication systems for cardiac tissues, engineering minimally invasive 4D nano-cell vehicles for the alleviation of patient discomfort during surgery and myocardial tissue regeneration is still in its infancy. Moreover, it will be ideal to develop a cellularized patch for cell therapy that prevents myocardial necrosis, restores the function of damaged tissues, and provides sufficient mechanical support to reduce the risk of ventricular remodeling. Considering a two-in-one strategy, the fabricated 4D structure would fold before injection and recover its initial shape at the targeting region without cell loss after delivery.[34] In addition, the use of human-induced pluripotent stem cell-derived cardiomyocytes (hiPSC-CMs) offers many advantages, such as excellent versatility, steady reproducibility, and optimal sensitivity.[35–41]

In this proof of concept in vitro study, we utilized a thermo-responsive shape memory polymer (SMP) to fabricate a 4D smart minimally invasive cardiac cell vehicle, which could consequently transform into an in situ cardiac patch at the infarcted region of myocardial tissue. After optimization of the blending ratio of the components, the synthesized thermo-responsive 4D ink exhibited a shape transformation behavior at the human body temperature. The engineered 4D cardiac constructs with different micro/nanoscale printing patterns were fabricated to make them well integrated with the innate micro/nanoscale features of the native myocardial tissues, and their 4D functionalities were also investigated. Moreover, a 4D construct that possesses excellent biocompatibility with the completion of microscale surface coating would enhance the uniform distribution and growth of cardiac cells on its surface.

Materials and Methods

All solvents and reagents were purchased from Sigma-Aldrich (St. Louis, MO) unless otherwise specified.

4D Construct Fabrication Process

The fabrication process of our 4D constructs has two steps, which are: 1) fused deposition modeling (FDM)-based 3D printing of different infill patterns and 2) reusable polydimethylsiloxane (PDMS) molds for the 4D ink stamping as shown in Figure 1a. First, polylactic acid (PLA) constructs (20 mm × 2 mm × 20 mm) (L × W × H) with three different printing patterns, linear (LN), diamond (DA), and hexagonal (HX), were designed and 3D printed via computer-aided design (CAD) software and an FDM printer (MakerBot, Brooklyn, NY). Next, the PDMS molds were created in a petri-dish with the 3D printed PLA constructs to engrave the printing patterns by adding 20 mL of a blended PDMS solution at the weight ratio of 10:1 (Silicon elastomer: curing agent) (Dow Corning, Midland, MI). After solidification in an oven at 75 °C for 1 hour, the PLA constructs were removed to obtain the reusable PDMS molds with different patterns. After which, 400 μL of our 4D ink was extruded into each mold to fabricate 4D smart constructs.

Preparation of 4D Printing Ink and Fabrication

The 4D ink used in our study consisted of three major components, including bisphenol A diglycidyl ether (B), poly(propylene glycol) bis(2-amino propyl) ether (P), and decylamine (D), which performs as a monomer, cross-linker, and cross-linking modulator (Figure 1a), respectively.[5] The cross-linking mechanism is the nucleophilic ring-opening reaction of amino and

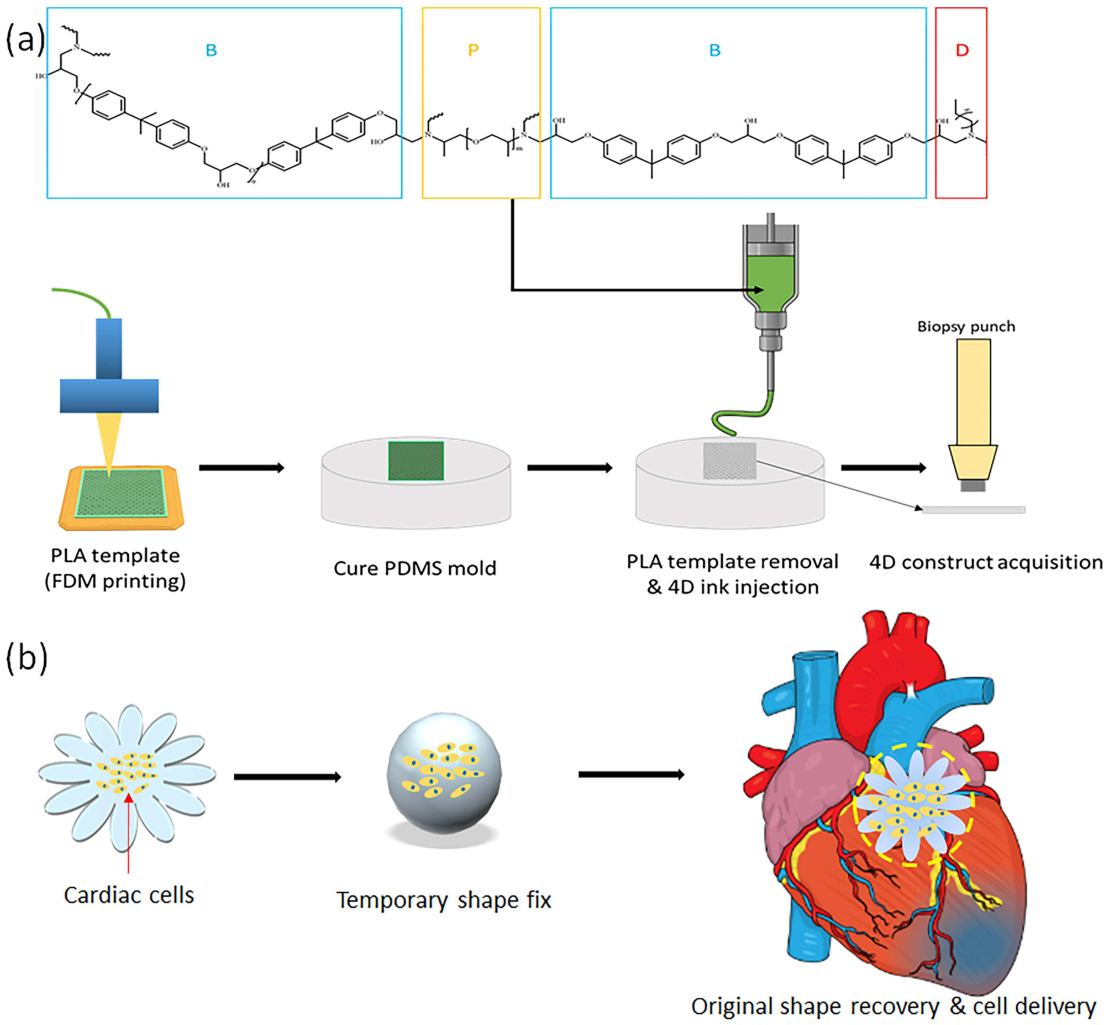

Figure 1 Schematic illustrations of (**a**) the fabrication steps of the 4D smart constructs and (**b**) the cell therapy process using the 4D construct (morphing from spherical cellularized vehicles to in situ curved tissue patch).

epoxy groups between these components. Each material was blended in a 15 mL centrifuge tube at the weight ratio of 3.4: 0.34: 1.15 at room temperature to obtain 4D shape-transformation behavior at the targeting temperature (~36 °C).[42] Following which, the ink was degassed in a vacuum chamber. The formulated 4D ink was stored at −80 °C and thawed in an oven at 75 °C for 5 mins prior to each use and extruded into the PDMS mold. The extrusion system was equipped with a 5 mL syringe and a blunt needle (1.6 mm diameter) to extrude 400 µL of the 4D ink into each PDMS mold at 1 mL/min flow rate. Then, the 4D constructs were further cured at 100 °C for 1 hour to complete the cross-linking process.[5] The constructs were then washed in deionized water (dH_2O) at 80 °C for 3 days and were subsequently placed in 70% (v/v) alcohol for an additional day to remove non-cross-linked residues.

Surface Morphology and Mechanical Property Characterization

The surface morphology of the 4D constructs was visually characterized by an FEI high-resolution Teneo LV Scanning electron microscope (SEM) (Zeiss, Oberkochen, Germany) after each sample was sputter-coated with a 3 nm layer of gold. Then, a 5 kV potential difference with a 13 pA electron beam was applied to the 4D constructs for imaging.[5,21]

To measure the tensile modulus of the 4D constructs, sample strips with the three different patterns at a dimension of 10 mm × 1 mm × 20 mm (L × W × H) were prepared. Before the tensile measurement was taken, the preload was set to 0.2 N, and the samples were tested at two different temperatures (25 °C and 45 °C, which is around ± 10 °C of the 4D actuation temperature) using an MTS Criterion testing system with a maximum 100 N load cell (MTS Systems Corp,

Eden Prairie, MN) at a speed of 1 mm/min until breakpoints.[21,43] For the compressive modulus test, 4D sample discs with the three different patterns at a dimension of 10 mm × 1 mm (D × H) were prepared. The samples were compressed at a strain rate of 1 mm/min (at 25 °C and 45 °C) with a preload of 0.01N to ensure initial contact between the loading plate and the samples. Then, the slope of the linear elastic region between 0 and 10% of the stress-strain curve was taken into account for the calculation of the compressive modulus.[21,43]

Measurement of 4D Shape-Changing Behavior

The thermo-responsive 4D shape-changing behavior of the fabricated 4D constructs was evaluated by precisely controlling the temperature of dH_2O in a water bath with the samples immersed. A 4D rectangular strip (50 mm × 10 mm × 1 mm) was prepared. The strip was first immersed in dH_2O at 36 °C (body temperature) and folded to a temporary "U" shape. Then it was left at room temperature for 1 min to fix the temporary shape, where the initial angle between the two parallel lines was marked as θ_i. To recover its original shape, the strip was transferred back into 36 °C dH_2O for 1 min, where the final angle was measured and marked as θ_f. Based on this measurement, the shape recovery rate (R) was calculated as follows.[26]

$$R = 100 - \left\{ \left(\frac{\theta_i - \theta_f}{\theta_i} \right) \times 100 \right\} (\%)$$

In addition, various shape-changing behaviors of different 4D samples were imaged and recorded using an iPhone 11 (Apple Inc., Cupertino, CA).

Cell Culture

Human-induced pluripotent stem cell-derived cardiomyocytes (hiPSC-CMs) were obtained from the National Heart, Lung, and Blood Institute at the National Institute of Health (Bethesda, MD) and cultured in the cardiomyocyte basic medium using the same protocol as previously reported studies.[5,44] The cells were incubated under standard culture conditions at 37 °C and 5% CO_2 concentration, and the media was changed daily.

Cell Proliferation and Morphology Analysis

To enhance cell adhesion and growth, a surface coating with Matrigel® (Corning Inc., Corning, NY) was performed on the fabricated 4D construct before the initial cell seeding process. Briefly, Matrigel® was added to the cell culture medium at a concentration of 11.1 μL/mL at 4 °C. Then, 300 μL of the mixed solution was added into a 48-well plate to entirely immerse 4D samples. The samples were incubated overnight under the same standard culture conditions to complete the surface coating process.

For hiPSC-CM proliferation studies, the cells were seeded at a density of 3×10^5 cells/cm^2 on the 4D samples, and the cell proliferation was quantified after 1, 4, and 7 days. On each day of the quantification, the cell-adhered 4D samples were rinsed three times with phosphate-buffered saline (PBS) to wash away non-adherent cells on the surface. After that, 400 μL of a cell counting solution, which consisted of 10% (v/v) cell counting kit solution (CCK-8, Dojindo Molecular Technologies, Japan) and 90% (v/v) hiPSC-CM culture media, was added to each well. Then, 200 μL of supernatant from each well was collected and transferred into a 96-well plate, and spectrophotometrically quantified using a Multiskan GO Spectrophotometer (Thermo Fisher Scientific, Waltham, MA) at 450 nm.[21,43]

To visually evaluate the cell viability and growth, a live-dead cell staining kit (BioVision, San Francisco, CA) was used following the enclosed protocol, and cell morphology analysis was performed using F-actin staining after 1 week of culture. Specifically, each 4D construct with seeded hiPSC-CMs was rinsed with PBS, and the adhered cells were fixed and permeabilized in 10% formalin and 0.1% Triton X-100 for 15 mins, respectively. The cytoskeleton of the cells was stained with Texas red™-X phalloidin dye in red for 1 hour, and the cell nuclei were stained with 4,6-diamidino-2-phenylindole dihydrochloride (DAPI) (Invitrogen, Carlsbad, CA) in blue for 5 mins, respectively. The stained cells were imaged using a Zeiss LSM 710 confocal microscope (Carl Zeiss AG, Oberkochen, Germany).[21,43]

Immunofluorescent Staining

Immunofluorescent staining was performed after 1 week of cell culture to explore the bioactivity of hiPSC-CMs on the 4D structure. Briefly, the adhered cells were fixed and permeabilized sequentially in 10% formalin and 0.1% Triton X-100 for 15 mins and immersed in 1% bovine serum albumin (BSA) blocking buffer to block non-specific antibody binding. Then, the cells were rinsed with PBS and stored at 4 °C overnight with the primary antibodies, ie, anti-sarcomeric alpha-actinin (α-actinin) (ab137346) (Abcam, Cambridge, UK) and anti-cardiac troponin I (cTnI) (sc-365446) (Santa Cruz Biotechnology, Dallas, TX). The next day, the adhered cells were rinsed with PBS and stained with the secondary antibodies, ie, Alexa Flour™ 488 goat anti-rabbit IgG H&L and Alexa Flour™ 594 goat anti-mouse IgG H&L (Thermo Fisher Scientific, Waltham, MA) in the dark at room temperature for 1 hour. Additionally, the cell nuclei were stained using DAPI for 5 mins. Likewise, images were obtained and analyzed using the confocal microscope.

Statistical Analysis

All quantitative data are presented as the mean ± standard deviation (n=9). Data were analyzed by one-way analysis of variance (ANOVA) with Student's *t*-test to verify statistically significant differences among experimental groups. A p-value <0.05 was considered to be statistically significant.[21]

Results

Fabrication and Surface Characterization of 4D Cardiac Constructs

The thermo-responsive 4D cardiac constructs with three different micro-patterns (LN, DA, and HX) were fabricated to replicate the anisotropic structure of native myocardial fibers using an FDM printer and a PDMS stamping mold, as illustrated in Figure 1. To print the three patterns with PLA filaments, the infill density of the FDM printer was set at 50% after optimization, ensuring an ideal manufacturing resolution of the final 4D constructs. The 4D SMP-based construct could exhibit a shape change behavior at its glass transition temperature (T_g), which was designated at body temperature (~36 °C) to secure the viability and bio-function of hiPSC-CMs after seeding. To obtain a shape transformation effect at our targeted temperature, the aforementioned optimal molar ratio for the B, P, and D were used to form the smart thermo-responsive ink.[42] Briefly, the sequential mechanism of our 4D shape transformation is as follows. First, when the 4D construct is exposed to an environment with a temperature higher than T_g, its temporary shape can be obtained by applying an external force and fixed at a temperature lower than T_g, which is specified herein as the thermomechanical programming step. Then, the 4D construct can recover its original shape once sufficient heat is provided to reach the temperature above T_g.[5,23,24]

Based on the created CAD files (Figure 2a–c), the surface morphologies of the fabricated 4D construct with the three different printing patterns (LN, DA, and HX) were studied using an SEM, as shown in Figure 2d–f. In the acquired images, the regularly aligned patterns and the detailed surface characteristics were visually observed.

Mechanical Properties of 4D Thermo-Responsive Materials

The tensile and compressive moduli for the 4D samples exhibited different results at 25 °C and 45 °C that are approximately below and above 10 °C of our targeting temperature (~36 °, which is also T_g of our 4D SMPs). It was shown that the tensile moduli of the LN, DA, and HX strips were ~149.91 MPa, ~173.98 MPa, and ~138.67 MPa at 25 °C, respectively. However, the tensile moduli of each group were decreased to ~116.53 MPa, ~142.67 MPa, and ~97.80 MPa when the temperature increased to 45 °C. A similar phenomenon was observed in the compression test. Specifically, the compressive moduli of the 4D discs changed from ~1577.09 MPa (LN), ~1682.66 MPa (DA), and ~1482.67 MPa (HX) to ~1449.50 MPa (LN), ~1452.68 MPa (DA), and ~1385.40 MPa (HX), respectively (Figure 3a and b).

Characterization of 4D Thermos-Responsive Behaviors

To investigate the thermo-sensitive shape memory capability of the fabricated 4D constructs, the strip was fixed in a temporary "U" shape after immersing it in dH_2O at 36 °C and transferring back to room temperature sequentially. Then, the shape recovery speed was measured at two different temperatures, 36 °C and 45 °C, until there was no further change.

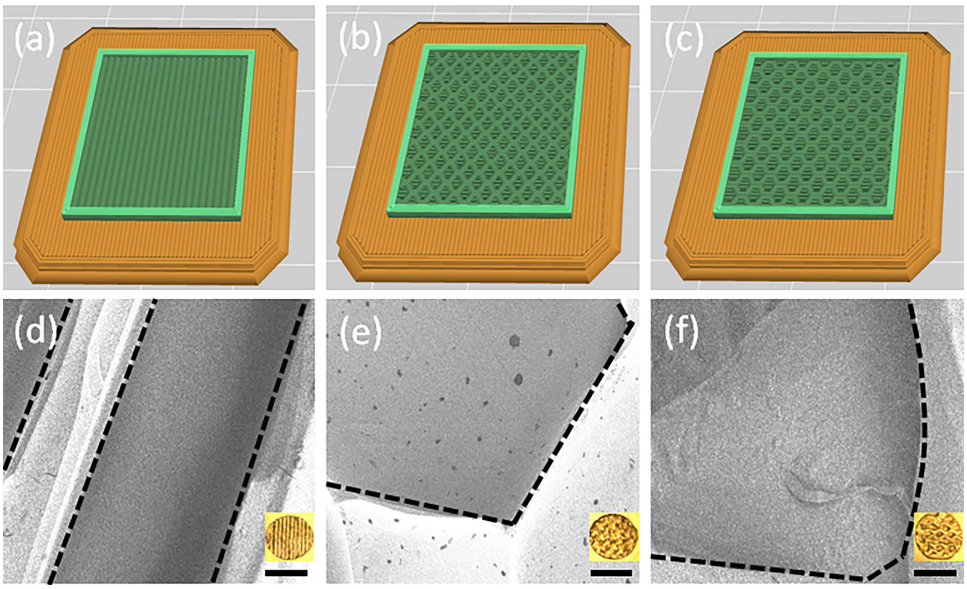

Figure 2 CAD images (STL) of the 4D disc constructs with (**a**) LN, (**b**) DA, and (**c**) HX patterns. SEM and photo images of the 4D constructs with different printing patterns, including (**d**) linear (LN), (**e**) diamond (DA), and (**f**) hexagonal (HX). Scale bars, 100 μm for SEM and 1 mm for photo images.

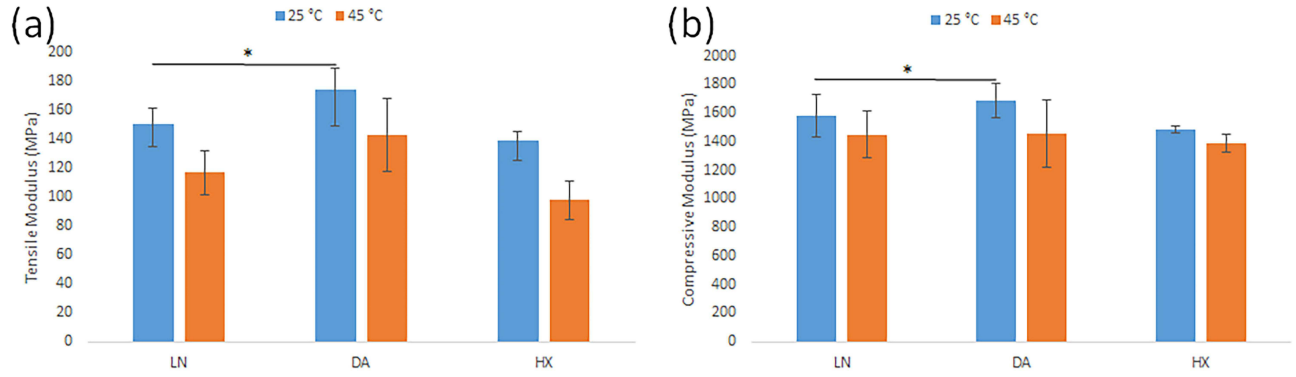

Figure 3 (**a**) Tensile moduli of the 4D strips with the three different printing patterns at 25 °C and 45 °C. (**b**) Compressive moduli of the 4D discs with the three different printing patterns at 25 °C and 45 °C. Data are the mean ± standard deviation; n=9, *p<0.05.

As shown in Figure 4a, the time required to recover the original shape of the 4D strip was shorter at a higher temperature. For the 4D strip with our ink, around 35 seconds were required to complete the shape recovery at 36 °C, whereas the same sample fully recovered its original shape in approximately 25 seconds at 45 °C. The entire shape recovery process of the 4D strip at T_g was consecutively imaged and recorded in Figure 4b and Supplementary Video 1.

Additionally, the thermo-responsive ability of the 4D construct was further explored to create cube- and sphere-shaped vehicles. As shown in Figure 5a and b, the initial 2D flat constructs were folded to fix temporary shapes, ie, a cube and a sphere, at room temperature, and then recovered their original structures within 150 and 35 seconds after they were exposed to 36 °C (T_g). Owing to the faster response time, the sphere-shaped vehicles would serve as cardiac cell vehicles when hiPSC-CMs were grown on their surface.

hiPSC-CM Proliferation and Myocardial Maturation on 4D Cardiac Constructs

The proliferation of hiPSC-CMs on the 4D constructs was quantified over 7 days. As shown in Figure 6a, the seeded hiPSC-CMs demonstrated a favorable proliferation rate regardless of the surface patterns, and there was no remarkable difference between the 4D constructs and the control group, a 48-polystyrene well-plate, which is one of the most commonly used tools for cell culture. Moreover, the 4D constructs with the HX pattern have the highest proliferation rate

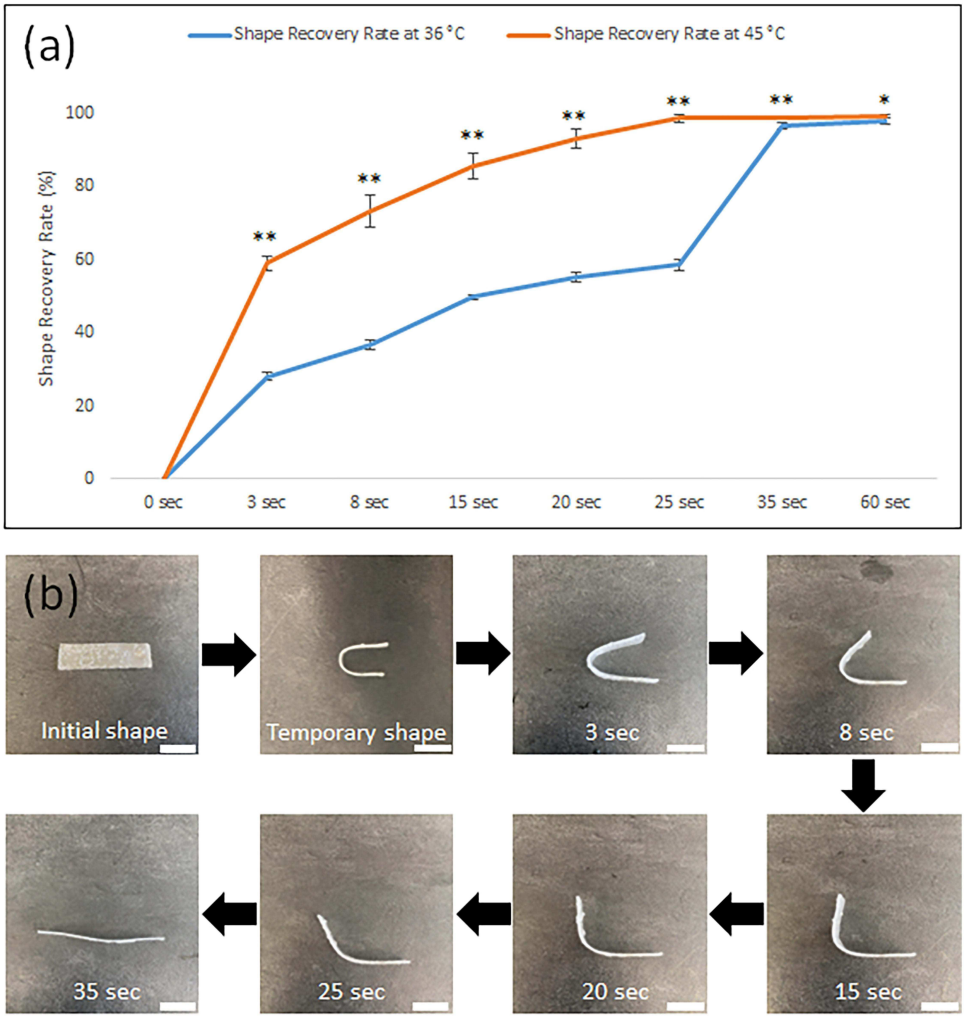

Figure 4 (**a**) The comparison of the shape recovery rate of the 4D strip at two different temperatures, 36 °C and 45 °C. Data are the mean ± standard deviation; n=9, *p<0.05 and **p<0.01 compared to the shape recovery rate data at 36 °C at each time point. (**b**) Sequential images of the shape recovery process of the 4D strip at 36 °C. Scale bars, 1 cm.

(avg. value) compared to other patterns. To visually observe the morphology of hiPSC-CMs, F-actin staining was performed on the 4D samples with different patterns after 7 days of culture (Figure 6b and c). Specifically, Figure 6b shows the uniformly distributed cells on the arched surface after shape transformation. It was also noticed that the cell distribution demonstrated the printing pattern-dependent spreading behavior and alignment compared to the control group, as shown in Figure 6c-i–c-iii and Figure S1a. Also, the cultured hiPSC-CMs showed a contractile function with a stable beating rhythm on the surface of the 4D construct after 7 days (Supplementary Video 2).

After optimization, the 4D construct with the HX pattern was used to evaluate the functionality of hiPSC-CMs. First, immunostaining with α-actinin and cTnI to detect and bind antibodies to myocardial-specific proteins was performed after 7 days of culture. The results exhibited stable myocardial protein expression of sarcomeric structure (α-actinin) and contractile protein (cTnI), as shown in Figure 6d-i–d-iii and Figure 6e-i–e-iii. To visually evaluate the cell viability, live-dead staining and the measurement of the contractile beating rate of hiPSC-CMs were performed until 7 days after seeding. It was demonstrated that the beating rate of the cells on the 4D scaffolds was slower due to the presence of the directional patterns on the 4D constructs, but more convergent and uniform than the hiPSC-CMs cultured on flasks (Figure 7a). It could be explained that the printing patterns on the 4D scaffolds provided hiPSC-CMs with an ideal environment that resembles the surface of the natural heart, which is advantageous as the cells maintain their stable contractile beating rate during the minimally invasive surgery process. Also, the hiPSC-CMs grown on the HX 4D constructs exhibited proper cell viability for up to 7 days of culture (Figure 7b-i–7b-iii, Figure 7c-i–7c-iii, and Figure S1b).

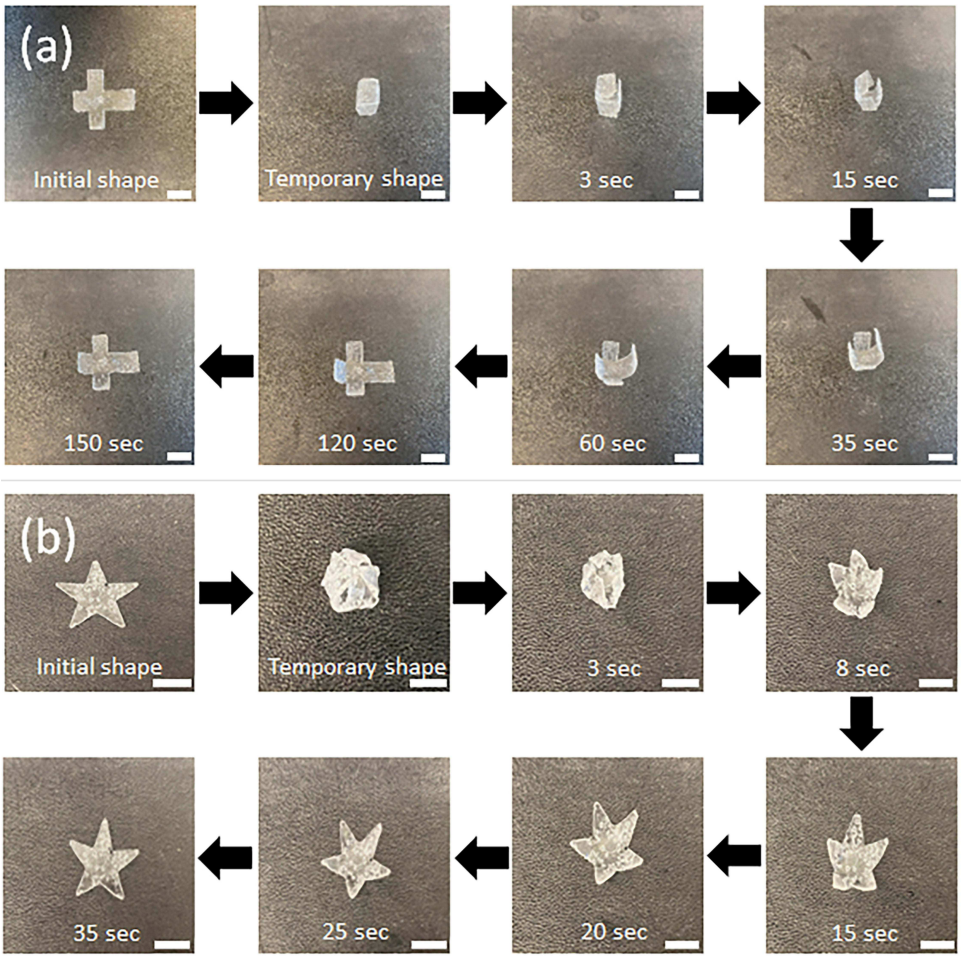

Figure 5 Sequential images of the shape recovery processes of the 4D constructs with (**a**) cubical and (**b**) spherical shapes until they restore their original shapes at 36 °C. Scale bars, 1 cm.

Discussion

The synthesized 4D SMP ink is an innovative candidate for the fabrication of smart 4D cardiac structures that integrate the functions of minimally invasive cell vehicles and in situ tissue patches using our two-in-one experimental design. The combination of 3D printing and a PDMS-based stamping mold enabled a fast and precise fabrication of the 4D constructs, given the direct extrusion printing of 4D SMP ink has relatively low resolution and reproducibility. As shown in Figure 2, the CAD (a-c), the SEM and photo images (d-f) demonstrated that our customized fabrication process could provide the regulated printing patterns in any dimensions, eg, geometries, infill densities, and widths, indicating our 4D constructs were precisely manufactured as we aimed to design.

The fabricated 4D scaffolds exhibited robust mechanical moduli and remarkable shape recovery capabilities at our targeting T_g of the polymerized smart-ink, which is close to human body temperature (~36 °C). It was observed that the fabricated 4D constructs exhibited different physical properties depending on applied temperatures. As shown in Figures 3 and 4a, the variation in moduli and shape recovery speed became more drastic with increasing temperature. Generally, SMPs experience a substantial change from a rigid to an elastic state once exposed to a designated stimulation,[45] and they provide a broad range of T_g from −70 °C up to 100 °C to permit their mechanical properties and shape recovery speed to vary depending on the temperature change.[45,46] Specifically, cross-linked thermoset polymers using covalent bonds are known to possess a greater mechanical modulus than thermoplastic elastomers.[26,47] The results demonstrated that our 4D materials had higher elasticity and stretchability to serve as myocardial patches for preventing post-infarction ventricular remodeling. Besides the shape recovery rate test using the 4D strip in Figure 4, continuous imaging of two typical 4D vehicles, such as a cube and a sphere (Figure 5), capable of transforming the

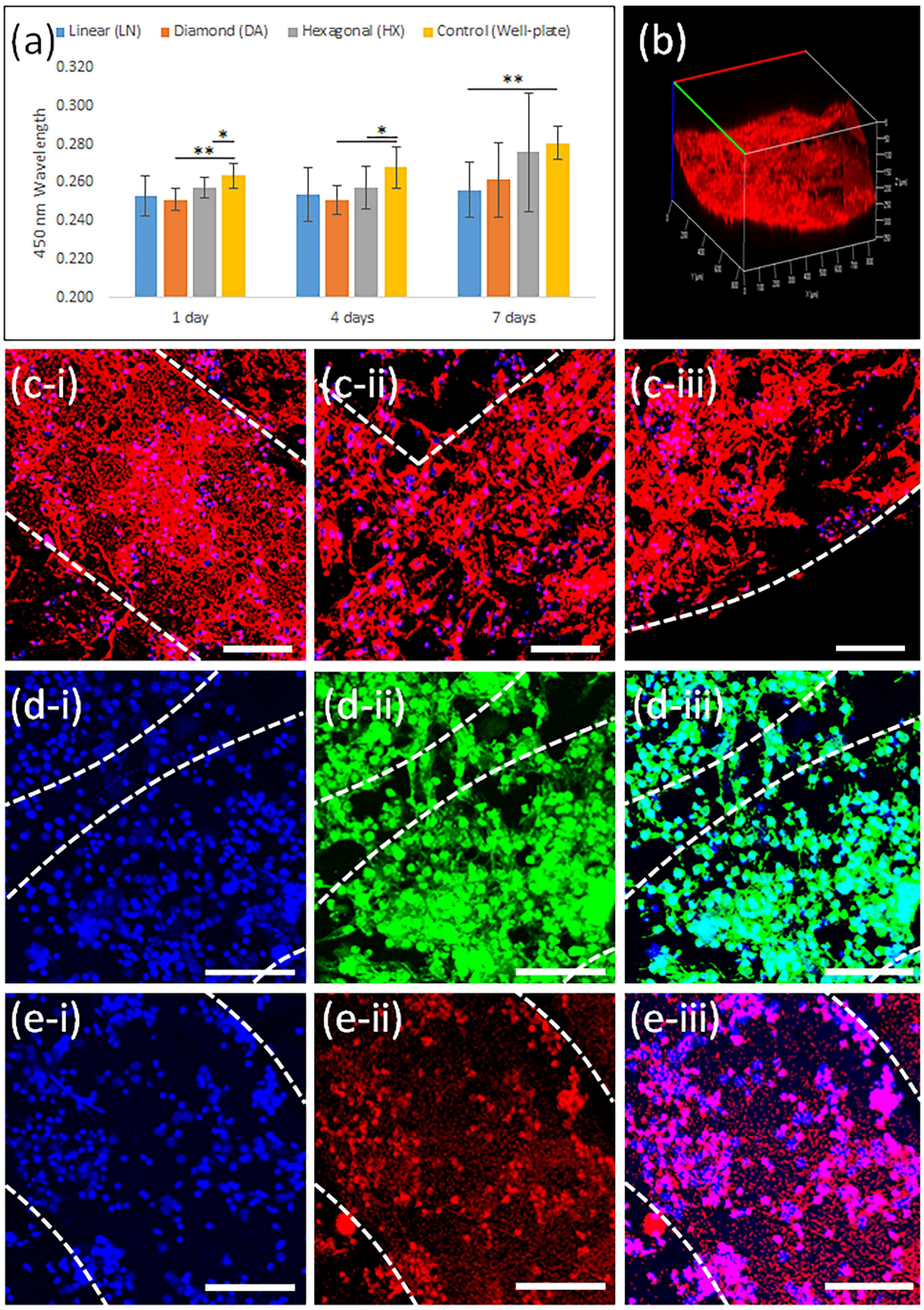

Figure 6 (**a**) The proliferation of hiPSC-CMs on the 4D constructs compared to a 48 well-plate after 1, 4, and 7 days. Data are the mean ± standard deviation; n=9, *p<0.05 and **p<0.01. (**b**) A confocal microscope image of evenly distributed hiPSC-CMs on the 4D construct after 4D shape transformation using F-actin staining. Confocal microscope images of F-actin stained hiPSC-CMs on the 4D constructs with (**c-i**) LN, (**c-ii**) DA, and (**c-iii**) HX printing patterns after 1 week of culture. Scale bars, 100 μm. Confocal microscope images of α-actinin stained hiPSC-CMs on the HX 4D constructs after 1 week of culture with (**d-i**) nucleus, (**d-ii**) cardiac-specific protein, and (**d-iii**) combined. Confocal microscope images of cTnI stained hiPSC-SMs on the HX 4D constructs after 1 week of culture with (**e-i**) nucleus, (**e-ii**) cardiac-specific protein, and (**e-iii**) combined. Scale bars, 100 μm.

cubical and spherical shape into unfolded patches, further demonstrated the outstanding thermo-responsive capabilities of our 4D materials for various shapes, Our 4D materials and fabricated scaffolds exhibit superior versatility regardless of their original shapes and dimensions, which is beneficial when designing minimally invasive cell vehicles for use in clinical conditions. The fast morphing of our 4D sphere-shaped constructs (spherical carriers) at the body temperature

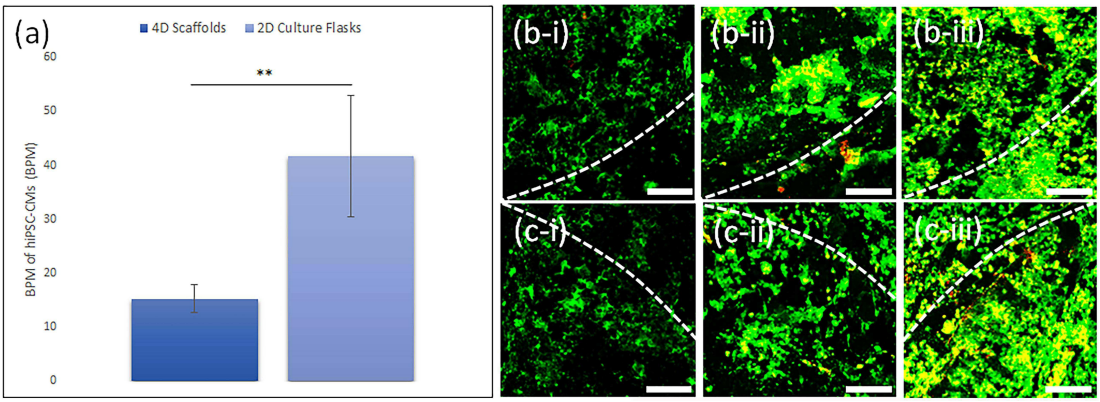

Figure 7 (**a**) Beating rate of hiPSC-CMs on the cell culture flasks and 4D constructs for 7 days. Data are the mean ± standard deviation; n=9 and **p<0.01. Confocal microscope images of live-dead assay stained hiPSC-CMs seeded on the HX 4D construct before its shape transformation on (**b-i**) day 1, (**b-ii**) day 4, and (**b-iii**) day 7. Confocal microscope images of live-dead assay stained hiPSC-CMs seeded on the HX 4D construct after its shape transformation on (**c-i**) day 1, (**c-ii**) day 4 and (**c-iii**) day 7. Scale bars, 100 μm.

illustrates their excellent ability in minimally invasive surgery. Moreover, the 4D construct became an elastomer-like patch (when above its T_g), which could perfectly cover the curved surface of myocardial tissue for flawless integration.

To develop a 4D smart construct, one of the most critical factors to consider is its biocompatibility with the designated cells. Although our 4D SMPs exhibit favorable biocompatibility, hiPSC-CMs require extremely strict culture conditions. Therefore, the post-surface coating process using Matrigel® significantly improved the adhesion and growth of hiPSC-CMs. More importantly, the seeded hiPSC-CMs at an initial density of 3×10^5 cells/cm^2 demonstrated a favorable cell proliferation rate, printing pattern-dependent alignment, and directional elongation on the surface of the 4D smart constructs over a week of culture (Figure 6a–c-iii). Additionally, the immunostaining results for the HX pattern, which is the most optimal design for our study due to cell proliferation (Figure 6a) as well as adaptability to ventricular curvature changes between diastole and systole,[25] illustrated the promoted sarcomere structure and myocardial maturation (Figure 6d-i–6d-iii and Figure 6e-i–6e-iii). Moreover, the stable and uniform contractile beating rate and live-dead staining results before and after 4D shape changes elucidated that the cell viability substantially increased over a week and the 4D transformation did not inhibit cell growth and beating functions (Figure 7a–c-iii), which supports the benefits of our 4D constructs in tissue engineering aspect. The results also showed that the printing pattern, initial shape, and morphing process of the 4D smart constructs have no substantial effect on the attachment and growth of cardiac cells.

The 4D bio-fabrication technique has gained considerable attention over the past decade since it theoretically enables the desired shape transformation on-demand. Based on which, the 4D technique can be an extremely attractive tool when used in unreachable areas of the human body, where the use of conventional biomedical approaches is limited.[23] As a means to deliver cardiac cells effectively to the targeted area, these novel 4D smart constructs that incorporate thermo-responsive SMPs into the cost- and time-effective 4D fabrication method which: 1) possesses superior biocompatibility with contractile cardiomyocytes to regenerate the myocardial tissue, 2) morphs rapidly from minimally invasive cell vehicles to in situ tissue patches at body temperature to deliver cardiac cells and restore cardiac functions, and 3) has high mechanical elasticity to prevent ventricular remodeling, have been successfully demonstrated for the first time. Our study provides an innovative concept of a 4D smart cardiac construct for the regeneration of myocardial tissues.

Conclusion

This study demonstrates a novel and innovative approach to fabricating a smart 4D thermo-sensitive cardiac construct for myocardial regeneration. Our 4D constructs present a precisely controllable transformation behavior with the presence of temperature change, which is utilized for achieving prompt self-morphing behavior from minimally invasive cell vehicles to in situ tissue patches promptly. Along with the optimal thermo-responsive 4D shape-change behavior, the results of the mechanical analysis, shape recovery, and cell study exhibit superior physical robustness as well as outstanding myocardial maturation on the fabricated 4D cardiac constructs. The present study will advance the current minimally

invasive cell delivery system and lead the utilization of 4D smart materials to the next stage of biomedical engineering applications. To advance the current study, in vivo transplantation will be further investigated to present its potential for future research in clinical trials.

Abbreviations

FDM, fused deposition modeling; hiPSC-CM, human-induced pluripotent stem cell-derived cardiomyocytes; SMP, shape memory polymer; PDMS, polydimethylsiloxane; PLA, polylactic acid; LN, linear; DA, diamond; HX, hexagonal; CAD, computer-aided design; B, bisphenol A diglyceryl ether; P, poly(propylene glycol) bis (2-amino propyl) ether; D, decylamine; dH_2O, deionized water; SEM, scanning electron microscope; PBS, phosphate-buffered saline; CCK-8, cell counting kit solution; DAPI, 4,6-diamidino-2-phenylindole dihydrochloride; BSA, bovine serum albumin; α-actinin, anti-sarcomeric alpha-actinin; cTnI, anti-cardiac troponin I.

Acknowledgments

The authors would like to thank the George Washington University Center for Microscopy and Image Analysis and the George Washington University Center for their assistance in image acquisition. The authors also thank Dr. Chengyu Liu and the iPSC core at the National Heart, Lung, and Blood Institute for providing hiPSC-CMs.

Funding

This work was supported by American Heart Association Transformative Project Award and NSF EBMS Program Grants 1856321 and 2110842.

Disclosure

The authors report no conflicts of interest in this work.

References

1. Virani SS, Alonso A, Aparicio HJ, et al. Heart disease and stroke statistics—2021 update: a report from the American Heart Association. *Circulation*. 2021;143(8):e254–e743. doi:10.1161/CIR.0000000000000950
2. Public Health Agency of Canada. Report from the Canadian Chronic Disease Surveillance System: Heart Disease in Canada, 2018. 2018.
3. Samuel M, Tardif J-C, Khairy P, et al. Cost-effectiveness of low-dose colchicine after myocardial infarction in the Colchicine Cardiovascular Outcomes Trial (COLCOT). *Eur Heart J Qual Care Clin Outcomes*. 2021;7(5):486–495. doi:10.1093/ehjqcco/qcaa045
4. Chen Q, Jin L, Cook WD, et al. Elastomeric nanocomposites as cell delivery vehicles and cardiac support devices. *Soft Matter*. 2010;6 (19):4715–4726. doi:10.1039/c0sm00213e
5. Wang Y, Cui H, Wang Y, et al. 4D printed cardiac construct with aligned myofibers and adjustable curvature for myocardial regeneration. *ACS Appl Mater Interfaces*. 2021;13(11):12746–12758. doi:10.1021/acsami.0c17610
6. Wei H-J, Chen C-H, Lee W-Y, et al. Bioengineered cardiac patch constructed from multilayered mesenchymal stem cells for myocardial repair. *Biomaterials*. 2008;29(26):3547–3556. doi:10.1016/j.biomaterials.2008.05.009
7. Cui H, Miao S, Esworthy T, et al. 3D bioprinting for cardiovascular regeneration and pharmacology. *Adv Drug Deliv Rev*. 2018;132:252–269. doi:10.1016/j.addr.2018.07.014
8. Ghasemi R, Moghaddam SI, Ramezani F, Yaghubi M. The effect of the door to needle time of streptokinase administration on the left ventricular function and Thrombolysis in Myocardial Infarction (TIMI) flow grade in patients with anterior myocardial infarction: a single-center, prospective follow-up study. *Acta Med Iran*. 2022;60(4):229.
9. Eshraghi A, Rezaei S, Yaghubi M. Risk factors of increased corrected TIMI frame count in angioplasty of culprit lesion after non-ST elevation acute coronary syndrome. *Arch Pharm Pract*. 2020;11:141–148.
10. Emmert MY, Hitchcock RW, Hoerstrup SP. Cell therapy, 3D culture systems and tissue engineering for cardiac regeneration. *Advanced Drug Deliv Rev*. 2014;69:254–269.
11. Peng X, Zhou J, Wu X-S. New strategies for myocardial infarction treatment. *J Cardiol Ther*. 2017;4(3):664–670. doi:10.17554/j.issn.2309-6861.2017.04.127
12. Parsa H, Ronaldson K, Vunjak-Novakovic G. Bioengineering methods for myocardial regeneration. *Adv Drug Deliv Rev*. 2016;96:195–202. doi:10.1016/j.addr.2015.06.012
13. Noor N, Shapira A, Edri R, Gal I, Wertheim L, Dvir T. 3D printing of personalized thick and perfusable cardiac patches and hearts. *Adv Sci*. 2019;6 (11):1900344. doi:10.1002/advs.201900344
14. Qiao L, Hu S, Liu S, et al. microRNA-21-5p dysregulation in exosomes derived from heart failure patients impairs regenerative potential. *J Clin Invest*. 2019;129(6):2237–2250. doi:10.1172/JCI123135
15. Torella D, Rota M, Nurzynska D, et al. Cardiac stem cell and myocyte aging, heart failure, and insulin-like growth factor-1 overexpression. *Circ Res*. 2004;94(4):514–524. doi:10.1161/01.RES.0000117306.10142.50

16. Alagarsamy KN, Yan W, Srivastava A, Desiderio V, Dhingra S. Application of injectable hydrogels for cardiac stem cell therapy and tissue engineering. *Rev Cardiovasc Med*. 2019;20(4):221–230.
17. Yoon SJ, Fang YH, Lim CH, et al. Regeneration of ischemic heart using hyaluronic acid-based injectable hydrogel. *J Biomed Mat Res B Appl Biomater*. 2009;91(1):163–171. doi:10.1002/jbm.b.31386
18. Waters R, Alam P, Pacelli S, Chakravarti AR, Ahmed RP, Paul A. Stem cell-inspired secretome-rich injectable hydrogel to repair injured cardiac tissue. *Acta Biomater*. 2018;69:95–106. doi:10.1016/j.actbio.2017.12.025
19. Wang L, Liu Y, Ye G, et al. Injectable and conductive cardiac patches repair infarcted myocardium in rats and minipigs. *Nat Biomed Eng*. 2021;5(10):1157–1173. doi:10.1038/s41551-021-00796-9
20. Hann SY, Cui H, Esworthy T, et al. Recent advances in 3D printing: vascular network for tissue and organ regeneration. *Transl Res*. 2019;211:46–63.
21. Hann SY, Cui H, Esworthy T, et al. Dual 3D printing for vascularized bone tissue regeneration. *Acta Biomater*. 2021;123:263–274. doi:10.1016/j.actbio.2021.01.012
22. Agarwal T, Fortunato GM, Hann SY, et al. Recent advances in bioprinting technologies for engineering cardiac tissue. *Mater Sci Eng C Mater Biol Appl*. 2021;124:112057.
23. Hann SY, Cui H, Nowicki M, Zhang LG. 4D printing soft robotics for biomedical applications. *Addit Manuf*. 2020;36:101567.
24. Cui H, Miao S, Esworthy T, et al. A novel near-infrared light responsive 4D printed nanoarchitecture with dynamically and remotely controllable transformation. *Nano Res*. 2019;12(6):1381–1388. doi:10.1007/s12274-019-2340-9
25. Cui H, Liu C, Esworthy T, et al. 4D physiologically adaptable cardiac patch: a 4-month in vivo study for the treatment of myocardial infarction. *Sci Adv*. 2020;6(26):eabb5067. doi:10.1126/sciadv.abb5067
26. Miao S, Zhu W, Castro NJ, et al. 4D printing smart biomedical scaffolds with novel soybean oil epoxidized acrylate. *Sci Rep*. 2016;6:27226. doi:10.1038/srep27226
27. YunáHann S, GraceáZhang L, KumaráMaiti T. 4D printing in biomedical applications: emerging trends and technologies. *J Mater Chem B*. 2021;9:7608–7632.
28. Miao S, Cui H, Nowicki M, et al. Photolithographic-stereolithographic-tandem fabrication of 4D smart scaffolds for improved stem cell cardiomyogenic differentiation. *Biofabrication*. 2018;10(3):035007. doi:10.1088/1758-5090/aabe0b
29. Serpooshan V, Hu JB, Chirikian O, Hu DA, Mahmoudi M, Wu SM. 4D printing of actuating cardiac tissue. In: *3D Printing Applications in Cardiovascular Medicine*. Elsevier; 2018:153–162.
30. Wang Y, Cui H, Esworthy T, Mei D, Wang Y, Zhang LG. Emerging 4D printing strategies for next-generation tissue regeneration and medical devices. *Adv Mater*. 2022;34(20):2109198. doi:10.1002/adma.202109198
31. Miao S, Castro N, Nowicki M, et al. 4D printing of polymeric materials for tissue and organ regeneration. *Mater Today*. 2017;20(10):577–591. doi:10.1016/j.mattod.2017.06.005
32. Ahmed A, Arya S, Gupta V, Furukawa H, Khosla A. 4D printing: fundamentals, materials, applications and challenges. *Polymer*. 2021;228:123926. doi:10.1016/j.polymer.2021.123926
33. Faruque MO, Lee Y, Wyckoff GJ, Lee CH. Application of 4D printing and AI to cardiovascular devices. *J Drug Deliv Sci Technol*. 2023;104162. doi:10.1016/j.jddst.2023.104162
34. Montgomery M, Ahadian S, Davenport Huyer L, et al. Flexible shape-memory scaffold for minimally invasive delivery of functional tissues. *Nat Mater*. 2017;16(10):1038–1046. doi:10.1038/nmat4956
35. Thomas D, Cunningham NJ, Shenoy S, Wu JC. Human-induced pluripotent stem cells in cardiovascular research: current approaches in cardiac differentiation, maturation strategies, and scalable production. *Cardiovasc Res*. 2022;118(1):20–36. doi:10.1093/cvr/cvab115
36. Burnett SD, Blanchette AD, Grimm FA, et al. Population-based toxicity screening in human induced pluripotent stem cell-derived cardiomyocytes. *Toxicol Appl Pharmacol*. 2019;381:114711. doi:10.1016/j.taap.2019.114711
37. Burridge PW, Diecke S, Matsa E, Sharma A, Wu H, Wu JC. Modeling cardiovascular diseases with patient-specific human pluripotent stem cell-derived cardiomyocytes. In: *Patient-Specific Induced Pluripotent Stem Cell Models*. Springer; 2015:119–130.
38. Blinova K, Stohlman J, Vicente J, et al. Comprehensive translational assessment of human-induced pluripotent stem cell derived cardiomyocytes for evaluating drug-induced arrhythmias. *Toxicol Sci*. 2017;155(1):234–247. doi:10.1093/toxsci/kfw200
39. Kawatou M, Masumoto H, Fukushima H, et al. Modelling Torsade de Pointes arrhythmias in vitro in 3D human iPS cell-engineered heart tissue. *Nat Commun*. 2017;8(1):1–11. doi:10.1038/s41467-017-01125-y
40. Sharma A, Burridge PW, McKeithan WL, et al. High-throughput screening of tyrosine kinase inhibitor cardiotoxicity with human induced pluripotent stem cells. *Sci Transl Med*. 2017;9(377):eaaf2584. doi:10.1126/scitranslmed.aaf2584
41. Strauss DG, Vicente J, Johannesen L, et al. Common genetic variant risk score is associated with drug-induced QT prolongation and torsade de pointes risk: a pilot study. *Circulation*. 2017;135(14):1300–1310. doi:10.1161/CIRCULATIONAHA.116.023980
42. Miao S, Cui H, Esworthy T, et al. 4D self-morphing culture substrate for modulating cell differentiation. *Adv Sci*. 2020;7(6):1902403. doi:10.1002/advs.201902403
43. Hann SY, Cui H, Zalud NC, et al. An in vitro analysis of the effect of geometry-induced flows on endothelial cell behavior in 3D printed small-diameter blood vessels. *Biomater Adv*. 2022;137:212832. doi:10.1016/j.bioadv.2022.212832
44. Lin Y, Linask KL, Mallon B, et al. Heparin promotes cardiac differentiation of human pluripotent stem cells in chemically defined albumin-free medium, enabling consistent manufacture of cardiomyocytes. *Stem Cells Transl Med*. 2017;6(2):527–538. doi:10.5966/sctm.2015-0428
45. Pei E, Loh GH. Technological considerations for 4D printing: an overview. *Prog Addit Manuf*. 2018;3(1):95–107. doi:10.1007/s40964-018-0047-1
46. Erkeçoğlu S, Sezer AD, Bucak S. Smart delivery systems with shape memory and self-folding polymers. *Smart Drug Deliv Syst*. 2016;80:1–29.
47. Xie T. Recent advances in polymer shape memory. *Polymer*. 2011;52(22):4985–5000. doi:10.1016/j.polymer.2011.08.003